International Forum on Aeroelasticity and Structural Dynamics
IFASD 2024
17-21 June 2024, The Hague, The Netherlands

INTEGRATED AERODYNAMIC AND STRUCTURAL MEASUREMENTS OF THE GUST RESPONSE OF A HINGED FOLDING WINGTIP

Christoph Mertens[1], Anna Biancotto[1], Jurij Sodja[2] and Andrea Sciacchitano[2]

[1] Royal Netherlands Aerospace Centre
Anthony Fokkerweg 2, 1059 CM Amsterdam, The Netherlands

[2] Delft University of Technology, Faculty of Aerospace Engineering
Kluyverweg 1, 2629 HS Delft, The Netherlands

Keywords: wind tunnel testing, gust generator, optical measurement technology, particle image velocimetry, unsteady aerodynamics, flexible wing, active gust load alleviation

Abstract: The gust response of an active hinged folding wingtip device that is mounted on a flexible wing is studied in a wind tunnel experiment. The aeroelastic response of this wing to the flow disturbance produced by a gust generator in the wind tunnel is analyzed using an optical measurement system that facilitates simultaneous measurements of the structural response of the wing and the aerodynamic flow field around the wing. Based on these measurements, the dynamic aeroelastic interaction can be characterized without requiring the instrumentation of the investigated wing model with sensors. The aerodynamic measurements are performed by tracking flow tracer particles. This paper presents a preliminary analysis on how these measurements can be used to determine the unsteady lift distribution during the gust encounter. The structural measurements are performed by tracking markers on the wing surface and fitting a structural model to these measurements. In this paper, this approach is validated by comparing the results to reference data from installed sensors, showing a good agreement.

1 INTRODUCTION

Ultra-high aspect ratio wings are known to be beneficial for the aerodynamic efficiency of aircraft but not currently common in aviation beyond gliders [1]. The maximum aspect ratio that can be realized on commercial airliners is effectively limited by two main factors, which are operational requirements for the wingspan in ground handling and considerations for both the structural design and control system related to aero(servo)elasticity [2]. The use of hinged folding wingtips is a straightforward solution for the wingspan limitations of operational nature, as such is an established standard for lower aspect ratio military aircraft and has more recently also been successfully implemented in higher aspect ratio commercial aircraft [3]. Overcoming the problems related to aero(servo)elasticity has been shown to be more challenging, such that these are still the subject of currently ongoing research.

One promising technological solution for increasing the maximum achievable aspect ratio on commercial airliners is the active hinged folding wingtip device by Wilson et al. [4]. The concept of this device features an active hinge that, in contrast to conventional folding wings and wingtips,

can be released and locked during flight. This active feature offers advantages for the aircraft's maneuverability and for reducing peak loads during gust encounters; see, among others, the studies published in Refs. [5,6,7,8,9,10]. As it is evident from these studies, a significant amount of research for the maturation of the active folding wingtip technology over the last decade has been conducted in wind tunnel experiments, before ultimately focusing on flight testing. In this context, it is notable that only relatively rudimentary experimental measurement techniques have been used in the wind tunnel tests, such as tufts and a small number of installed sensors (potentiometer, accelerometers, strain gauges). The use of these simple experimental techniques can be justified as part of a time- and cost-effective wind test campaign; however, on the other hand, their use neglects the significant potential of modern wind tunnel measurement technology for generating deeper physical insights during the technological maturation process.

Optical measurement techniques for wind tunnel testing have undergone significant developments in recent years, nowadays allowing the volumetric measurement of time-resolved flow fields for aeronautics research using particle image velocimetry [11]. A considerable advantage of these measurements is not only the amount of aerodynamic information that is obtained, but also the fact the measurements are performed without using installed sensors, which simplifies the experimental model design. Equivalent approaches for structural measurements are the longer established photogrammetry [12] and digital image correlation techniques [13]. More recently, it has been shown that optical structural measurements can also be performed together with aerodynamic measurements using a Lagrangian particle tracking technique in an integrated approach [14]. However, applications of this approach to aeroelasticity have so far been limited to steady and periodic aeroelastic phenomena [15,16].

In the present study, the integrated structural and aerodynamic measurement approach based on optical measurements is applied to the gust response of an active hinged folding wingtip mounted on a flexible wing in a wind tunnel experiment. This is the first application of the approach to a fully unsteady, transient aeroelastic phenomenon. The analysis of the structural measurements is adapted from the existing analysis approaches without requiring significant modifications, although improved accuracy may be obtained when increasing the fidelity of the employed structural model. The unsteady aerodynamic analysis on the other hand is significantly hampered by the limited number of flow tracer particles in the flow field and therefore restricted to a steady analysis for this paper.

2 WIND TUNNEL EXPERIMENT

2.1 Wind tunnel and gust generator

The experiment is conducted in the W-Tunnel at Delft University of Technology. The W-Tunnel is an open test section, open return wind tunnel, which is equipped with a square nozzle exit measuring $0.4\ \mathrm{m} \times 0.4\ \mathrm{m}$. At the nozzle exit of the wind tunnel, a gust generator with a cross-sectional area of $0.35\ \mathrm{m} \times 0.4\ \mathrm{m}$ is mounted. The gust generator features two vertical vanes that are actuated to produce a "$1 - \cos$" gust in the open test section. For the present study, the gust frequency is $f_g = 8\ \mathrm{Hz}$, and the pitch amplitude of the gust vanes is $\alpha_g = 2.5°$, reproducing the test conditions at which the gust load alleviation of the active folding wingtip has previously been shown to be effective in Ref. [10]. The wind tunnel is operated to produce a freestream velocity of $U_\infty = 10\ \mathrm{m/s}$ in the test section.

2.2 Hinged folding wingtip model and instrumentation

The experimental model of this study is mostly identical to the wing model that is described in detail in Ref. [10], specifically the wing labeled as "wing C" in that study, which has the highest stiffness. The wing is an untapered and unswept wing with a chord length of $c = 100$ mm and a span width of $s = 700$ mm, featuring a NACA 0018 profile. The folding wingtip hinge is located at the spanwise position 500 mm from the wingroot and has a flare angle of $\Lambda = 15°$. The wing dimensions are shown in Fig. 1.

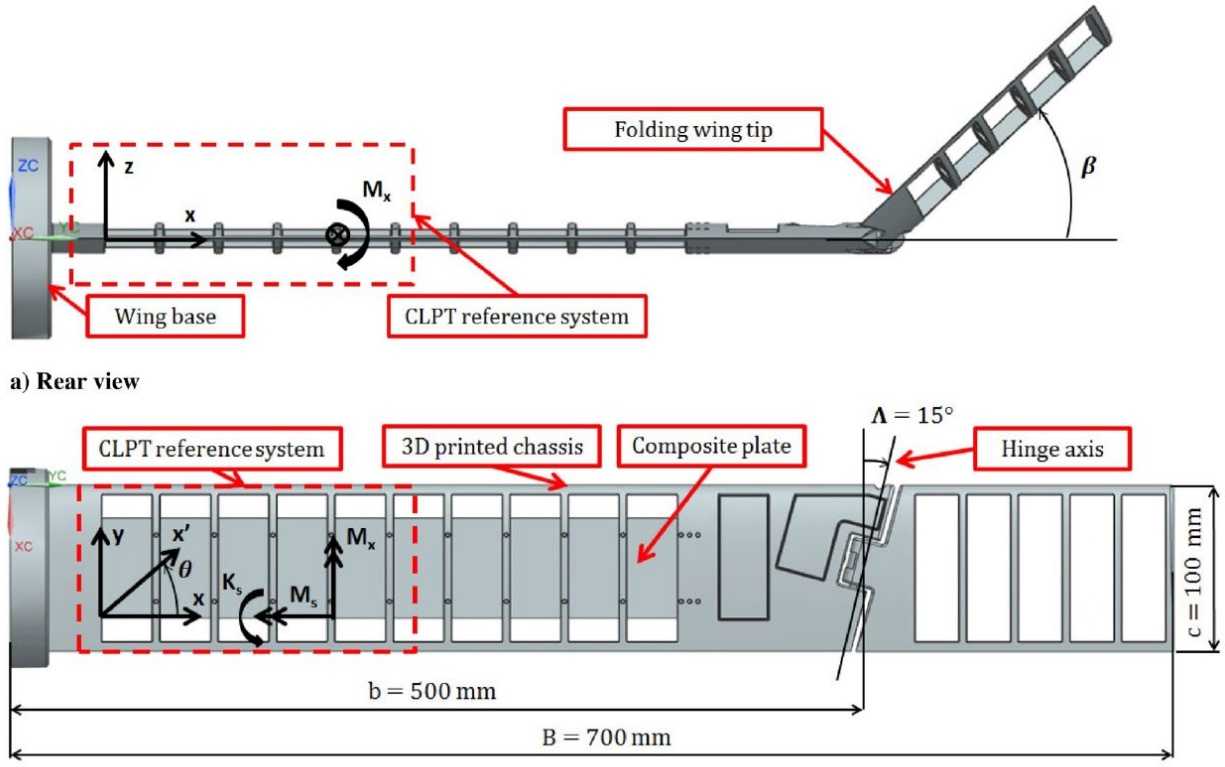

Figure 1: CAD model of the wing with indication of dimensions, from the wing design study in Ref. [10].

The wing is equipped with a servomotor that actuates the hinge release at a pre-selected timing with respect to the incoming gust. In this study, the hinge is released at the time instant when the gust arrives at the leading edge of the wing. Furthermore, the wing features strain gauges to measure the root bending moment and a potentiometer to measure the relative fold angle β. For more detailed information about the wing design, the reader is referred to Ref. [10].

An alteration of the wing design for the present study with respect to the previous studies is the application of a pattern of circular markers with white paint on the otherwise non-reflective black surface of the wing, constituted by a thin foil. These markers have a diameter of approximately 1.5 mm and are used for the optical tracking of the structural motion. Four markers are placed in the chordwise direction with a spacing of 30 mm (following the curvature of the wing surface) on both sides of the wing at several spanwise locations. On the folding wingtip, the spanwise spacing is 30 mm, resulting in six rows of markers. On the main wing, the spanwise marker spacing is decreased to 15 mm to compensate for the fact that the main wing is not a rigid body and only partly in the field of view of the optical measurement system.

The wing with the marker pattern as mounted in the wind tunnel for the experiment is shown in Fig. 2. The wing is mounted vertically, with the folding wingtip at the bottom. This configuration reduces the impact of the mass of the wingtip on the gust response characteristics of the wing, as discussed in detail in Ref. [10]. The wing is set to a geometric angle of attack of $\alpha = 5°$ with respect to the freestream and placed $200\ \mathrm{mm}$ downstream of the gust generator, with the wingtip $100\ \mathrm{mm}$ above the bottom of the gust generator exit to account for the shear layer. Note that this setup implies that the larger part of the main wing is not experiencing any inflow, only the wingtip is fully placed in the wind tunnel stream. While this setup choice affects the significance of the results for direct comparisons with numerical simulation data, it is identical to the setup in Ref. [10] and sufficient for the purpose of this demonstration study of the measurement approach.

Figure 2: Wing model with folding wingtip mounted vertically in the test section, with an upstream view of the gust generator and the turbulence grid inside the wind tunnel nozzle.

2.3 Optical measurement setup

The optical measurements in this experiment are performed with a set of six synchronously operated Photrom Fastcam high-speed cameras, acquiring images at a rate of $2700\ \mathrm{Hz}$. The six cameras are installed in such a way that measurements on both sides of the wing can be obtained simultaneously, with three cameras mounted on each side of the wing with different viewing angles to facilitate the volumetric measurements. All cameras are calibrated in the same coordinate system using a two-sided calibration plate before installing the wing. The illumination is provided by two LaVision LED-Flashlight 300 units. These units are mounted on both sides of the wing on top of the test section and operated in pulse mode, synchronized with the cameras by a LaVision Programmable Timing Unit. To increase the amount of illumination, particularly in the wingtip region further away from the light sources, a mirror is placed beneath the test section, outside of the field of view of the cameras. The setup for the optical measurements is shown in Fig. 3.

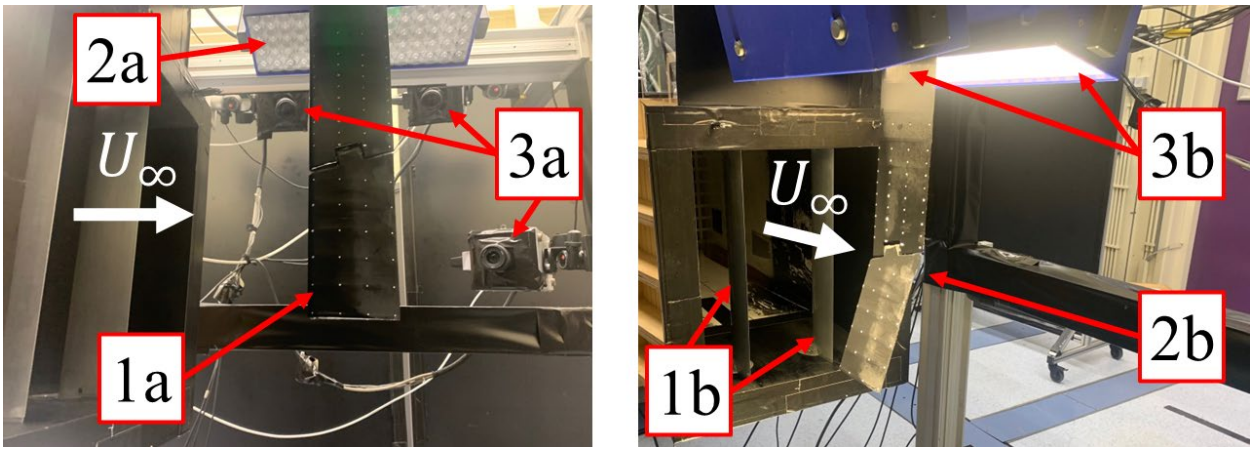

(a) (b)

Figure 3: Photos of the experimental setup. (a) View from the side, 1a: wing with folding wingtip device, 2a: LED flashlight (off), 3a: three high-speed cameras, (b) view from downstream, 1b: gust generator, 2b: wing with the folding wingtip released, 3b: illumination provided by two LED flashlights.

The optical structural measurements are performed by imaging the circular markers on the wing surface. For the aerodynamic measurements, the flow is seeded with neutrally-buoyant HFSB tracer particles. For this purpose, a seeding generator grid is installed in the wind tunnel, upstream of the wind tunnel contraction. The seeding generator features HFSB-producing 200 nozzles distributed over a cross-sectional area of $950\ \text{mm} \times 450\ \text{mm}$. These dimensions are not sufficient to cover the entire wind tunnel cross section, which is the reason why the turbulence grid was installed, to enhance mixing of the HFSB in the freestream and thereby increase the width of the achievable flow field measurement volume. The measurement volume that is obtained is approximately cubic, with dimensions of $300\ \text{mm} \times 300\ \text{mm} \times 300\ \text{mm}$, where the wingtip is located at the bottom edge of the measurement volume and the wing's spanwise axis approximately in the center of the volume for the streamwise and crossflow directions.

3 DATA PROCESSING AND ANALYSIS METHODS

3.1 Optical measurements data processing

The acquired image data is processed with the LaVision DaVis 10 software. A schematic flow chart of the data processing steps is shown in Fig. 4. At the center of the data processing is the Lagrangian particle tracking algorithm "Shake-the-box" [17], which computes particle positions and velocities (and accelerations) for both structural markers and flow tracers from the image data. Prior to the application of the Lagrangian particle tracking algorithm, the image data is pre-processed. The pre-processing begins with the separation of the acquired image into two data sets, one per each side of the wing. This is done because the DaVis 10 software was found to have difficulties analyzing image datasets measured from different viewing angles, with different regions of the field of view obstructed by the wing. Note that this step does not significantly hamper the following steps in the data analysis because the 6 cameras could be calibrated in the same coordinate system, such that the separately processed results from the two sides can be easily combined again into one dataset. Following this initial step, the image data processing employs the same approach as in previous studies [14,15,16], which is also briefly described in the following.

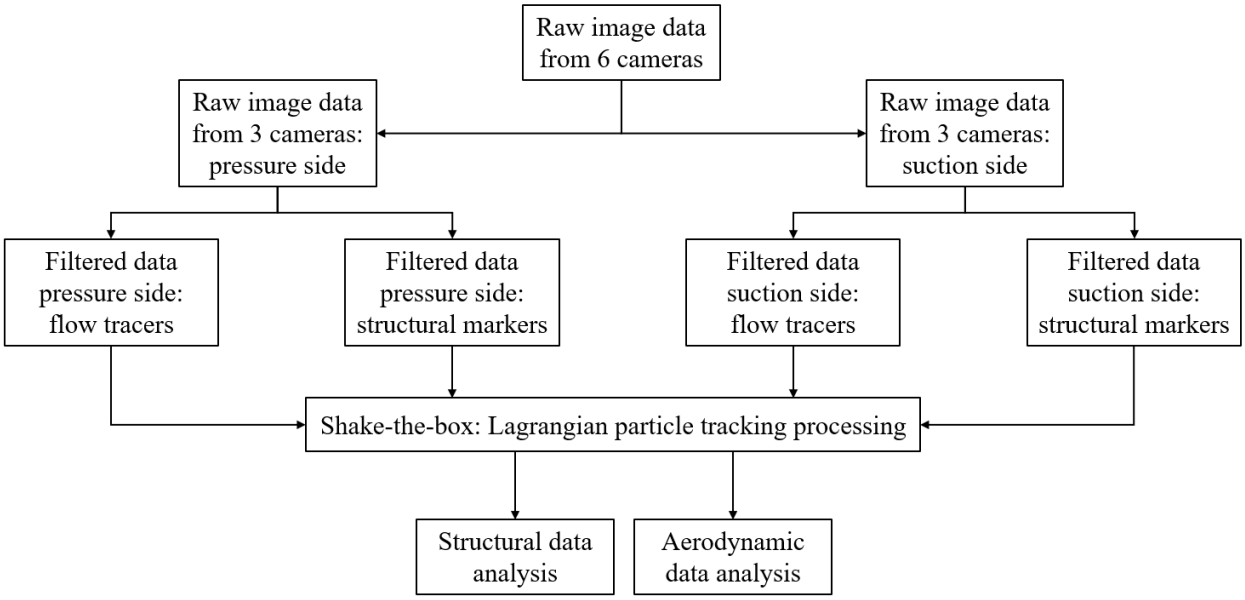

Figure 4: Optical measurement data processing flow chart

After the split of the dataset into the pressure and suction sides, an identical image filtering procedure is applied to both. The purpose of the image filtering is to separate the structural markers and the flow tracers, so that they can analyzed separately. This is required because the size and brightness of the markers is different from the flow tracers in the images, which means that optimal performance of the Lagrangian particle tracking algorithm is only achieved when they are analyzed separately. The filtering that is performed is a temporal filter applied to the time series of the images, where a low-pass filter isolates the structural information and a high-pass filter isolates the flow tracers, as shown exemplary in Fig. 5. The Lagrangian particle tracking analysis is then performed for the four datasets, two per side and for both structure and flow. Based on the datasets that results from this, the structural and aerodynamic data analyses that are described in the following two subsections are performed.

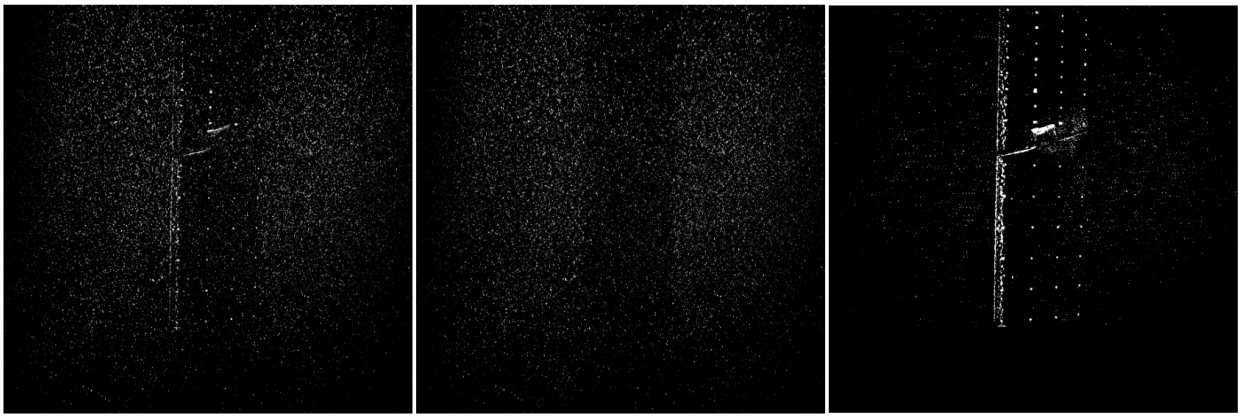

(a) **(b)** **(c)**

Figure 5: Image filtering example: (a) raw image, (b) high-pass filtered image, (c) low-pass filtered image

3.2 Structural data analysis

The structural data analysis begins with a coordinate transformation of the marker position measurements from the measurement coordinate system to the wind tunnel coordinate system. The six degrees of freedom of this coordinate transformation are determined by performing an optimization, where marker position measurements of the undeformed wing (wind tunnel off) are matched to the known marker positions that were painted on the wing. The wind tunnel coordinate system has its origin at the leading edge of the root of the wing, with x being the streamwise direction and z as the spanwise direction.

After the measurement data is transformed into the wind tunnel coordinate system, a structural model is used to reconstruct the wing shape from the marker measurements under loaded conditions. A simple structural model is used, based on an Euler-Bernoulli beam model for the spanwise axis of the main wing (assuming small bending deformations and neglecting torsion) and a rigid body model for the folding wingtip. The structural analysis can be further simplified by making assumptions on the loading of the wing. If it is assumed that the wing is loaded only on the wingtip and not on the main wing due to the wind tunnel setup, and that the loading on the wingtip is evenly distributed (seen as tip force and moment by the main wing), then the structural model can be used to represent the deformed wing shape based on only two parameters, the wingtip folding angle relative to the deformed position and inclination of the hinge, and the root bending moment. These two parameters can then be experimentally determined by performing a best fit optimization between the marker position measurements. Figure 6 shows the results of the model fit to the marker position measurements for steady inflow conditions.

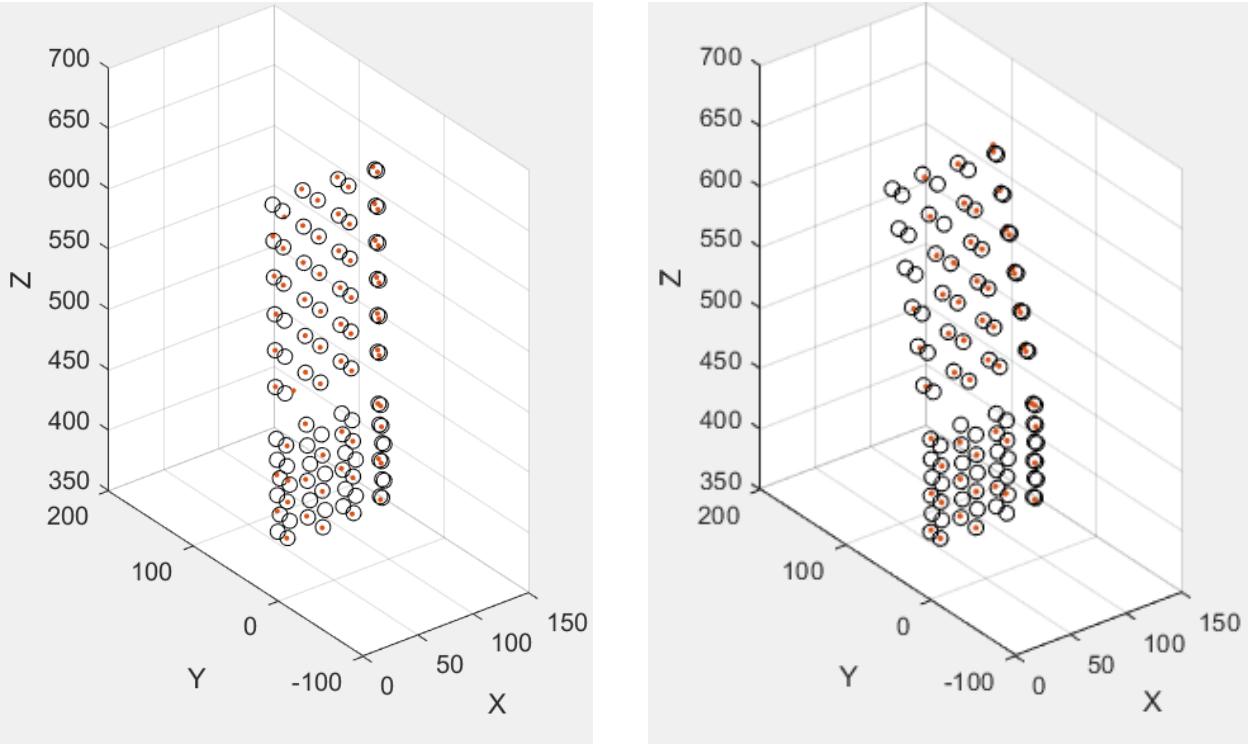

(a) **(b)**

Figure 6: Visualization of particle position measurements (red dots) with best fit for the structural model (black circles) for steady inflow conditions. (a) locked hinge, (b) unlocked hinge. Dimensions are in mm.

For the structural analysis of the wing's response to the gust inflow, the same model is used as for the steady cases, thereby neglecting the inertial force due to motion of the main wing. This is justified by considering that the motion amplitudes (and thus accelerations) of the main wing are much smaller than those of the winglet, which are accounted for through the variable tip force on the main wing.

3.3 Aerodynamic data analysis

The aerodynamic data that is obtained in terms of individual flow tracer particle positions and velocities is ensemble-averaged [18] into a volumetric flow field. For the present study, a bin size of 10 mm × 10 mm × 10 mm with an overlap of 50% is used. One section of the flow field for steady inflow conditions with locked hinge is shown in Fig. 7, with an indication of the wing position using the marker-based shape reconstruction. Remarkable about this flow field measurement is the clearly visible wake of the gust generator vanes at around $y = 110$ mm and $y = -70$ mm. Also indicated in the figure is an elliptic contour, which is used to determine the circulation Γ around the wing. This is done by interpolating the flow field along the elliptic path and then performing a line integration along the path. Using the Kutta-Zhukovski theorem, the section lift can be estimated from the circulation: $L' = \rho\, U_\infty\, \Gamma$. Because the wind tunnel does not cover the entire wing span, not only the circulation but also the freestream velocity needs to be determined experimentally per wing section to calculate the lift, which is done by extracting the measured flow velocity approximately 100 mm upstream of the wing.

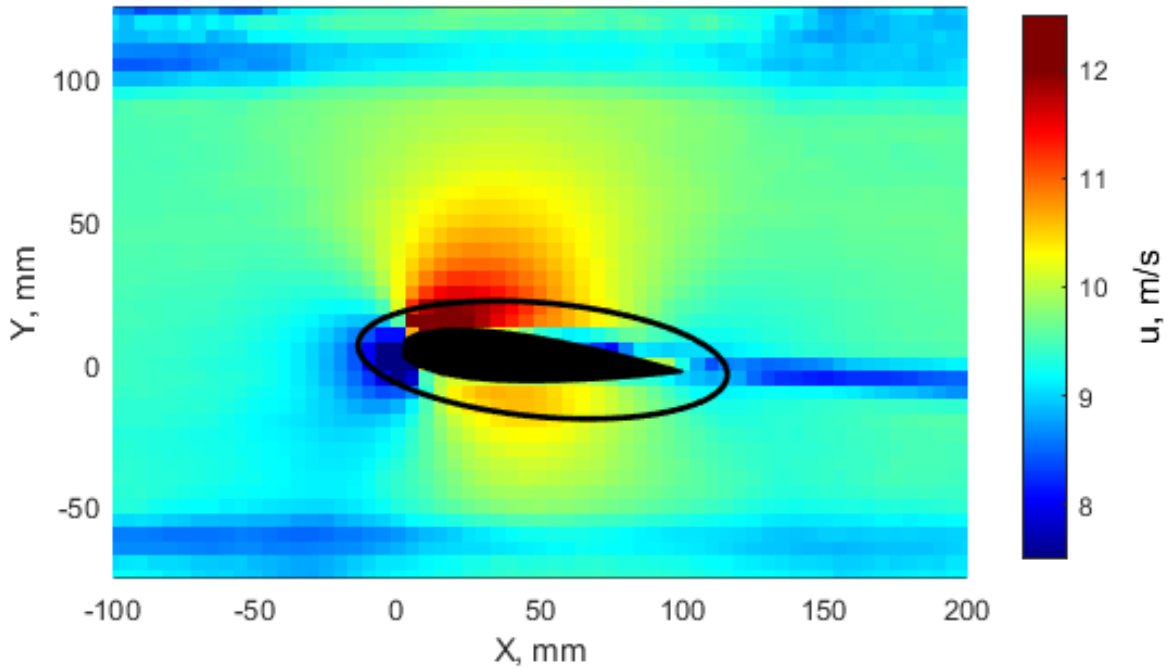

Figure 7: Section of the measured flow field for steady inflow with locked hinge at Z = 550 mm, with an indication of the wing section and an elliptic contour for the circulation determination.

In this paper, the unsteady flow field data that is measured during the gust encounter could not be analyzed; instead, it is demonstrated that the same ensemble-averaging method that is used for the steady data is unsuited for the analysis of unsteady flow field data.

4 RESULTS

4.1 Structural response to steady inflow and gust response

The structural analysis method is first validated by comparing the wing root bending moment coefficient that is obtained for steady inflow with locked hinge with the reference value based on the measurements with the strain gauges, which is $C_{RBM,sensor} = 0.0170$. When both degrees of freedom of the structural model are fitted to the marker position measurements, a fold angle of $\beta_{markers} = 0.72°$ and a moment coefficient of $C_{RBM,markers} = 0.0139$ are obtained. The agreement of this result with the sensor measurement is somewhat improved as the value reaches $C_{RBM,markers} = 0.0165$ when the wingtip folding degree of freedom is manually fixed to be zero, considering the locked hinge. However, the agreement of both results with the sensor-based result can be regarded as satisfactory, considering the rudimentary structural model that is used.

After the first assessment of the method for steady inflow, the structural response is analyzed for two gust response test cases. The first test case, in which the hinge remains locked, is shown in Fig. 8, and the second case, where the hinge is released when the gust arrives at the leading edge, is shown in Fig. 9. The qualitative and quantitative agreement is overall good, the differences in magnitude of the root bending moment between the sensor-based and the marker-based data is similar to the steady test case. The difference between potentiometer measurements and the marker-based fold angle result remains within 1°, which is satisfactory. Qualitative differences between the two methods are mainly the higher noise levels in the sensor data, and the presence of small-scale oscillations after the gust has passed, which are not captured by the optical measurement approach.

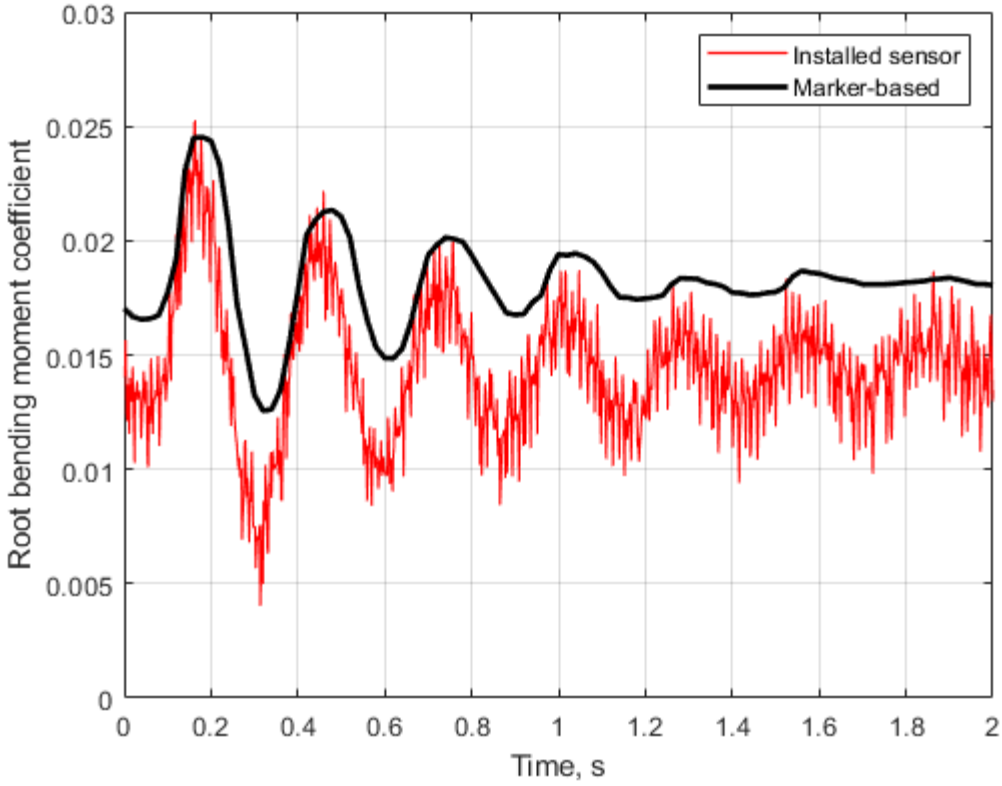

Figure 8: Comparison between the structural response measurements from installed sensors with the marker-based approach during a gust encounter with locked hinge.

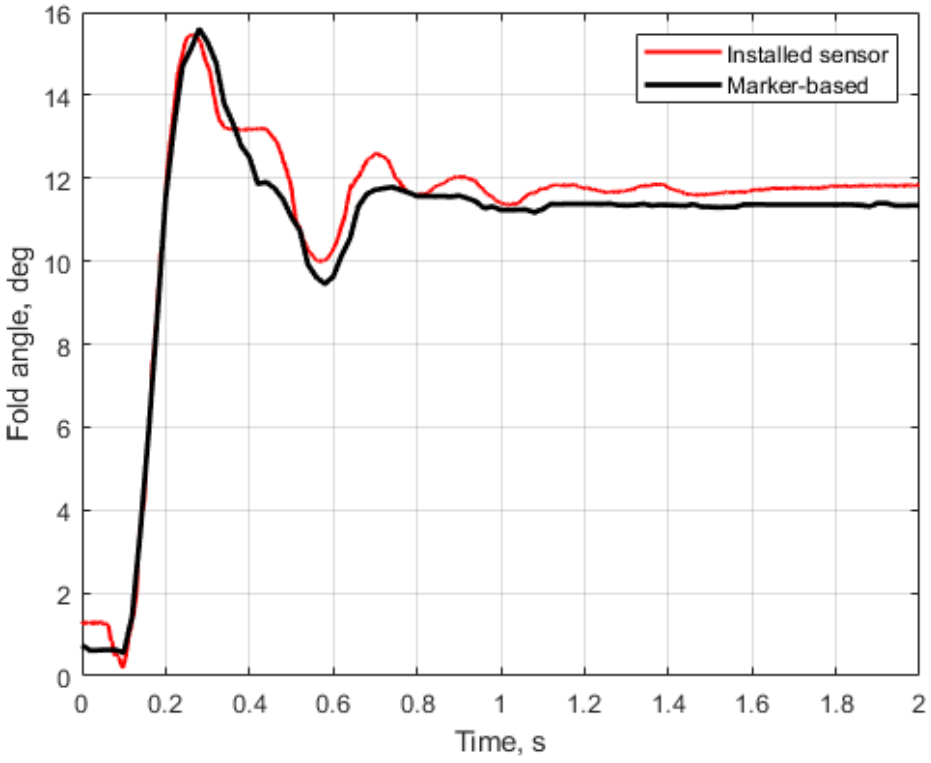

(a)

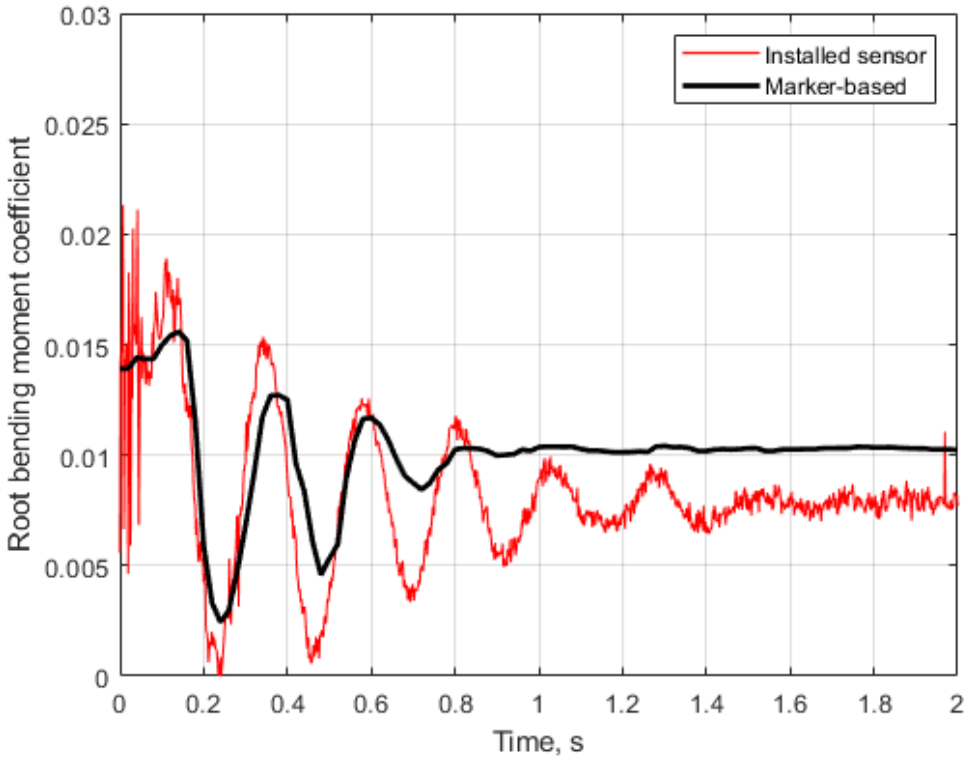

(b)

Figure 9: Comparison between the structural response measurements from installed sensors with the marker-based approach during a gust encounter with hinge release. (a) wingtip fold angle, (b) root bending moment.

A further noticeable difference between the sensor- and marker-based results is a phase shift in the results for the root bending moment. One potential explanation for this phase shift is the use of the quasi-steady structural model, neglecting the inertia effects of the main wing, potentially causing a phase shift with respect to the quasi-steady model which produces results relating to the temporal behavior of the deformation only.

4.2 Lift determination for steady inflow

The first result of the aerodynamic analysis related to the lift determination is the sensitivity of the circulation to the selection of the elliptic integration contour. For this purpose, the ellipse is described in terms of two parameters, the streamwise semi-axis length a and the semi-axis length b in the crossflow direction. The results for the circulation as both of these parameters are varied is shown in Fig. 10.

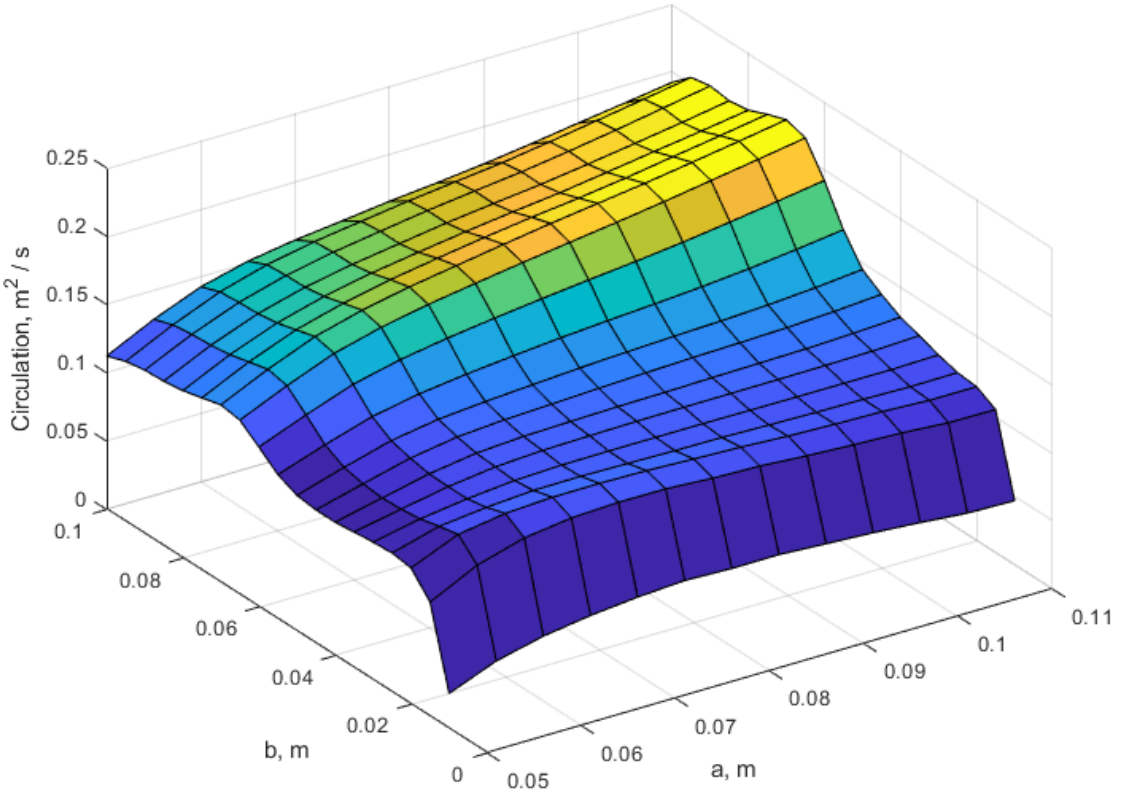

Figure 10: Variation of the circulation as depending on the parameters of the ellipse, for Z = 550 mm.

In an ideal potential flow field, the circulation is independent of the integration contour, as long as the entire wing section is enclosed. In real flows, viscous effects, three-dimensional effects and measurement resolution issues may affect the results particularly close to the wing surface, as it is also evident in Fig. 10 for the smallest values of a and b. In the present case, it is furthermore visible that the circulation increases significantly for larger values of b and particular combinations of large values for a and b. The explanation for this observation is the presence of the viscous wake of the gust generator vanes in the flow field. It is therefore important to exclude any overlap between the circulation integration contour and the wake of the gust generator. This is best achieved by selecting a relatively small elliptic contour that is not in the immediate vicinity of the wing surface. For this study, $a = 70$ mm and $b = 30$ mm are selected.

When a suitable integration contour is identified, the lift can be determined for every spanwise station of the flow field along the wing and the lift distribution along the span is obtained. The result is shown with the black dashed line in Fig. 11. The lift distribution is characterized by a relatively sharp drop at the wingtip, a more gradual drop inboard due to shear layer of the wind tunnel nozzle and a lift deficit around $z = 500$ mm, which is where the presence of the hinge decreases the aerodynamic efficiency of the wing locally.

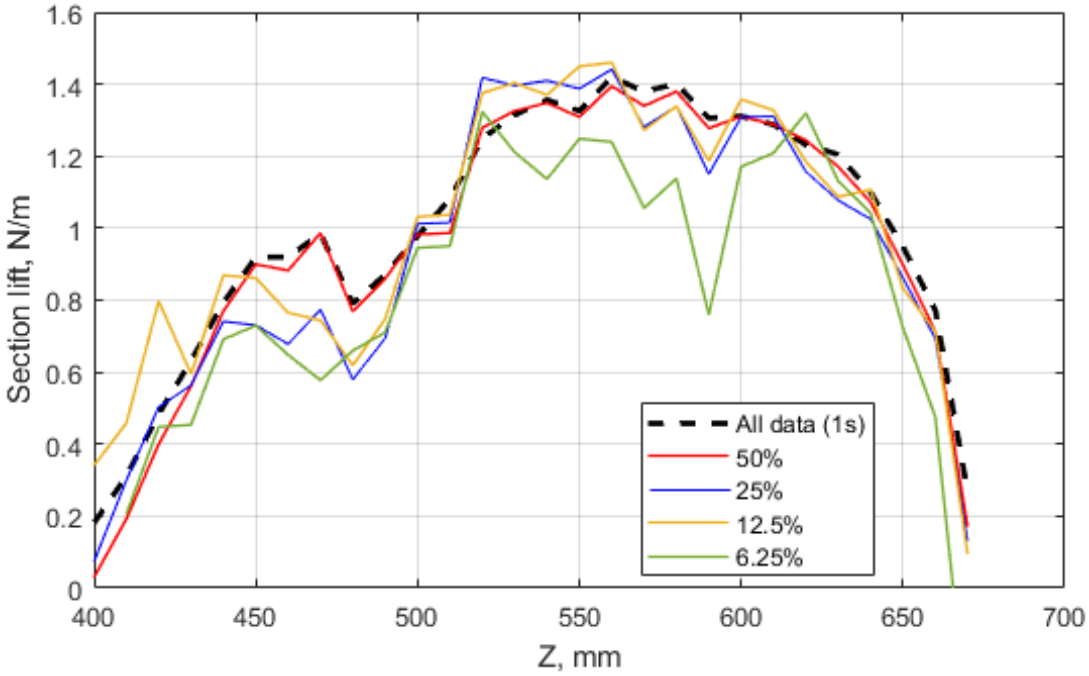

Figure 11: Spanwise lift distribution for steady inflow with locked hinge, with using different segments of the time series of the acquired image data for the analysis.

Figure 11 also shows the lift distribution that results when the amount of input data is reduced. For the considered steady inflow case, 1 s of data (2700 images) was acquired. The different colored lines in the graph show the effect on the obtained lift distribution when the number of images (and corresponding acquisition time) is halved four times. The impact on the lift distribution results is considerable for the smaller time segments, for 6.25% the overall lift is erroneously reduced by more than 20%. It must be noted here that 6.25% corresponds to a measurement duration of 62.5 ms, which is still much too long to resolve the gust response with a gust duration of 125 ms.

5 CONCLUSION AND OUTLOOK

In this paper, the gust response of an actively released hinged folding wingtip mounted on a flexible wing has been analyzed experimentally. A wind tunnel experiment was performed where the structural and aerodynamic behavior of the wing was measured with an integrated optical approach. The analysis of the structural measurements has been shown to be relatively straightforward, showing a good agreement with reference data from installed sensors even when using a rudimentary structural model for the analysis. The aerodynamic analysis has been found to be more challenging, while the lift distribution on the wing could be determined based on the flow field measurements for steady inflow conditions, it was found that the number of tracked flow tracer particles is not sufficient to perform the same analysis for unsteady data.

Future studies should focus on developing technical solutions for increasing the number of flow tracer particles in the wind tunnel experiment and/or using improved approaches for the aerodynamic load determination that are more robust to the much smaller number of tracer particles when performing an unsteady analysis. The capability to perform unsteady aerodynamic analyses is an important target in the further development of the integrated measurement approach used in this study, such that it can be effectively used in maturation studies of future aircraft technologies.

ACKNOWLEDGEMENT

The experiment presented in this paper has been conducted by the first author together with Fabio Taccaliti and Xavier Carillo Córcoles, whose contribution is gratefully acknowledged.

REFERENCES

[1] Anderson Jr., J. D., Fundamentals of Aerodynamics (5th edition). *McGraw-Hill*, 2011.

[2] Ma, Y., Elham, A., Designing high aspect ratio wings: A review of concepts and approaches. *Progress in Aerospace Sciences*, 2024, *145(100983)*.

[3] Smith, M. H., Renzelmann, M. E., and Marx, A. D., U.S. Patent Application for "Folding Wing-Tip System," The Boeing Company, Seattle, Washington, Docket No. 5,381,986 A, filed 17 Jan. 1995.

[4] Wilson, T., Herring, M., Pattinson, J., Cooper, J., Castrichini, A., Ajaj, R., and Dhoru, H., An Aircraft Wing with Moveable Wing Tip Device for Load Alleviation, (International Patent No. WO2017/118832Al). *World Intellectual Property Organization*, Jul. 13, 2017.

[5] Castrichini, A., Hodigere Siddaramaiah, V., Calderon, D., Cooper, J., Wilson, T., and Lemmens, Y., Nonlinear Folding Wing Tips for Gust Loads Alleviation. *Journal of Aircraft*, 2016, *53(5)*.

[6] Cheung, R. C., Rezgui, D., Cooper, J. E., and Wilson, T., Testing of a hinged wingtip device for gust loads alleviation. *Journal of Aircraft*, 2018, *55(5)*.

[7] Cheung, R. C., Rezgui, D., Cooper, J. E., and Wilson, T., Testing of folding wing-tip for gust load alleviation in high aspect ratio wing. *AIAA Scitech 2019 Forum* (paper no. 1863).

[8] Healy, F., Cheung, R., Neofet, T., Lowenberg, M., Rezgui, D., Cooper, J., Castrichini, A. and Wilson, T., Folding wingtips for improved roll performance. *Journal of Aircraft*, 2022, *59(1)*.

[9] Healy, F., Cheung, R., Rezgui, D., Cooper, J., Wilson, T., and Castrichini, A., Experimental and numerical nonlinear stability analysis of wings incorporating flared folding wingtips. *Journal of Aircraft,* 2024, *61(1).*

[10] Carillo Córcoles, X., Mertens, C., Sciacchitano, A., van Oudheusden, B. W., De Breuker, R., and Sodja, J., Effect of Wing Stiffness and Folding Wingtip Release Threshold on Gust Loads. *Journal of Aircraft,* 2023, *60(6)*.

[11] Wolf, C. C., Schwarz, C., Kaufmann, K., Gardner, A. D., Michaelis, D., Bosbach, J., Schanz, D., & Schröder, A., Experimental study of secondary vortex structures in a rotor wake. *Experiments in Fluids*, 2019, *60(175).*

[12] Liu, T., Burner, A. W., Jones, T. W., & Barrows, D. A., Photogrammetric techniques for aerospace applications. *Progress in Aerospace Sciences*, 2012, *54(1–58)*.

[13] Pan, B., Digital image correlation for surface deformation measurement: Historical developments, recent advances and future goals. *Measurement Science and Technology*, 2018, *29(082001).*

[14] Mertens, C., Sciacchitano, A., van Oudheusden, B. W. and Sodja, J., An integrated measurement approach for the determination of the aerodynamic loads and structural motion for unsteady airfoils. *Journal of Fluids and Structures*, 2021, *103(103293).*

[15] Mertens, C., de Rojas Cordero, T., Sodja, J., Sciacchitano, A. and van Oudheusden, B. W., Aeroelastic Characterization of a Flexible Wing Using Particle Tracking Velocimetry Measurements. *AIAA Journal*, 2022, *60(1).*

[16] Mertens, C., Costa Fernández, J. L., Sodja, J., Sciacchitano, A. and van Oudheusden, B. W., Nonintrusive Experimental Aeroelastic Analysis of a Highly Flexible Wing. *AIAA Journal,* 2023, *61(7).*

[17] Schanz, D., Gesemann, S., and Schröder, A., Shake-the-box: Lagrangian particle tracking at high particle image densities. *Experiments in Fluids*, 2016, *57(7).*

[18] Agüera, N., Cafiero, G., Astarita, T., and Discetti, S., Ensemble 3D PTV for high resolution turbulent statistics. *Measurement Science and Technology*, 2016, *27(124011)*.

COPYRIGHT STATEMENT

The authors confirm that they, and/or their company or organisation, hold copyright on all of the original material included in this paper. The authors also confirm that they have obtained permission from the copyright holder of any third-party material included in this paper to publish it as part of their paper. The authors confirm that they give permission, or have obtained permission from the copyright holder of this paper, for the publication and public distribution of this paper as part of the IFASD 2024 proceedings or as individual off-prints from the proceedings.